The influence of carbon impurities on the formation of loops in tungsten irradiated with self-ions

Castin, N.

2019-12-15

Castin , N , Dubinko , A , Bonny , G , Bakaev , A , Likonen , J , De Backer , A , Sand , A E , Heinola , K & Terentyev , D 2019 , ' The influence of carbon impurities on the formation of loops in tungsten irradiated with self-ions ' , Journal of Nuclear Materials , vol. 527 , 151808 . https://doi.org/10.1016/

http://hdl.handle.net/10138/334547
https://doi.org/10.1016/j.jnucmat.2019.151808

The influence of carbon impurities on the formation of loops in tungsten irradiated with self-ions.

N. Castin[1,*], A. Dubinko[1], G. Bonny[1], A. Bakaev[1], J. Likonen[2], A. De Backer[3], A.E. Sand[4], K. Heinola[4] and D. Terentyev[1]

[1] Studie Centrum voor Kerneenergie - Centre d'Étude de l'énergie Nucléaire (SCK•CEN), NMS unit, Boeretang 200, B2400, Mol, Belgium.
[2] VTT Technical Research Centre of Finland, P.O.Box 1000, FIN-02044 VTT, Finland
[3] CCFE, Culham Science Centre, Abingdon, Oxon, OX14 3DB, United Kingdom.
[4] Department of Physics, University of Helsinki – P.O. Box 43, FI–00014 Helsinki, Finland.

[*] Corresponding author: nicolas.m.b.castin@gmail.com

Abstract

The microstructure changes taking place in W under irradiation are governed by many factors, amongst which C impurities and their interactions with self-interstitial atoms (SIA). In this work, we specifically study this effect by conducting a dedicated 2-MeV self-ions irradiation experiment, at room temperature. Samples were irradiated up to 0.02, 0.15 and 1.2 dpa. Transmission electron microscopy (TEM) expectedly revealed a large density of SIA loops at all these doses. Surprisingly, however, the loop number density increased in a non-monotonous manner with the received dose. Performing chemical analysis with secondary ion spectroscopy measurements (SIMS), we find that our samples were likely contaminated by C injection during the irradiation. Employing an object kinetic Monte Carlo (OKMC) model for microstructure evolution, we demonstrate that the C injection is the likely factor explaining the evolution of loops number density. Our findings highlight the importance of the well-known issue of C injection during ion irradiation experiments, and demonstrate how OKMC models can help to rationalize this effect.

1 Introduction

Commercially pure rolled tungsten (W) is the baseline material selected for the plasma-facing components in the divertor of the ITER Tokamak thermonuclear facility [1]. The production of thermal energy from the fusion reaction will generate 14.1 MeV neutrons, releasing their energy within plasma-facing components. This process will inevitably lead to the formation of atomic collision cascades, and the creation of the lattice defects, whose size distribution and density will evolve during the reactor operation [2]. The formation of vacancies and nano-pores will result in the reduction of the thermal and electrical conductivity [3,4], induce dimensional instability (i.e., swelling) [5], and yield

to the retention of tritium [6]. These degradations, all together, are hence expected to reduce the performance of the fusion device. The formation of self-interstitial clusters growing into dislocation loops results in the hardening [4,7]. It therefore increases the ductile to brittle transition temperature [2,8], imposing a risk of structural failure during operation. The resulting microstructure depends on three key elements: (1) the irradiation conditions (i.e. flux, spectrum, fluence) generating lattice damage; (2) the intrinsic properties of the material (i.e. elastic constants) determining the structural morphology of the defects; (3) the material microstructure which controls diffusion and sinking of defects. Considering that the plasma facing components will be made of commercially pure tungsten, the presence of impurities such as carbon belongs to the last item. Due to strong interaction of carbon with vacancies and dislocations [9,10], even small traces of carbon can have strong impact on the resulting irradiation induce microstructure.

Physically-based modeling [11,12] can help to rationalize the complicated process of the irradiation damage accumulation and directly extrapolate its prediction to service conditions in term of neutron fluence and spectrum, irradiation temperature and its transients, dose rate, nuclear transmutation resulting to the formation of rhenium and osmium, etc. In recent works [9,10], we have proposed a complete object kinetic Monte Carlo (OKMC) model that takes all these factors into account. The model was developed, parameterized, and validated covering a wide temperature range (400-1000°C) and using a variety of the experimental conditions, namely: 2-MeV self-ions [13,14], 18-MeV self-ions [15] and JOYO material test reactor irradiation [16]. Satisfactory agreement was obtained for the number density and sizes of voids and dislocation loops applying a single-set input database.

Those computational works highlighted that one key aspect in the OKMC model is the description of self-interstitial (SIA) defects, and their interactions with C impurities. In this work, we combine an experimental and computational study to specifically study this aspect. For that purpose, we employed a simple non-activating irradiation setup at room temperature. This ensures that only SIA defects are mobile, while vacancy defects and carbon impurities do not diffuse [17, 18]. To avoid dealing with irradiation induce activation, we performed irradiation experiment employing 2MeV self-ions, for which the molecular dynamic database of collision cascades is well established. Combination of the low irradiation temperature and heavy ion damage yields to the microstructure composed of dislocation loops, which could be observed directly by transmission electron microscopy (TEM) already at such low dose as 0.02 dpa. We have exposed the samples to three levels of damage, up to 1 dpa. Next, we simulated this irradiation experiment with our OKMC tool to study how the observed densities/size distribution of the loops is influenced by the C impurities. Variable parameters are the effective carbon concentration in the bulk, and the strength of C-loop interaction. Additionally, we investigated the role of the increase of C concentration near the sample surface, as secondary ion spectroscopy measurements (SIMS) have indicated the injection of carbon during the irradiation. The latter is, today, a well-known issue for ion irradiation facilities [19-23].

2 Experimental procedure

2.1 Materials selection and samples preparation

We studied commercially pure W materials produced by Plansee AG, according to ITER specification [1]. The material was supplied as a bar with a square cross-section of 36 mm, fabricated by double forging.

Squared specimens (1 cm × 1 cm × 0.1 cm) for self-ion irradiation were prepared with electrical discharge machining (EDM) from the bulk. They were afterwards annealed at 1000 °C during one hour for stress relief purposes, and then polished with SiC papers up to P4000 and diamond suspension with 3 and 1 μm particle size.

The reference microstructure of this material was studied in Ref. [24]. Electron backscatter diffraction (EBSD) analysis revealed that the grains of this material are elongated along the bar axis. Those with high misorientation angles are randomly orientated and are elongated with a size of 5-20 μm in the normal direction to the bar axis, and 10-100 μm along the bar axis. Further analysis with Transmission electron microscopy (TEM) revealed sub-grain structures, which were also elongated with a size varying in the range 0.6-4 μm. The dislocation density is estimated to be 4.5×10^{12} m^{-2}.

After the self-ion irradiation, TEM samples were prepared by back-side thinning and polishing with SiC paper up to P4000, cutting with diamond wire saw, gluing to a TEM grid with a thermoplastic cement, electro-chemical polishing with a solution of 0.15 wt. % NaOH in water at a voltage set at 30 V.

2.2 Irradiation with self-ions

2-MeV W+ self-ions irradiation were performed in vacuum, at room temperature, with the TAMIA 5 MV Tandem accelerator of the University of Helsinki's ion beam laboratory. The W+ ion beam was raster scanned over the whole sample surface, and incoming ion flux was 1.37×10^{11} ions/cm^2/s.

Using the SRIM software [25], assuming a threshold displacement energy of 55.3 eV [26], we estimate that the depth of penetration is 0.35 μm, as illustrated in Fig. 1. The dose rate is estimated to be 2×10^{-3} dpa/s at the depth of maximum displacement, i.e., 100 nm. Three samples were irradiated at three different doses:

- Dose of 1.14×10^{12} ions/cm^2, which corresponds to 0.02 dpa
- Dose of 1.02×10^{13} ions/cm^2, which corresponds to 0.15 dpa
- Dose of 1.0×10^{14} ions/cm^2, which corresponds to 1.2 dpa

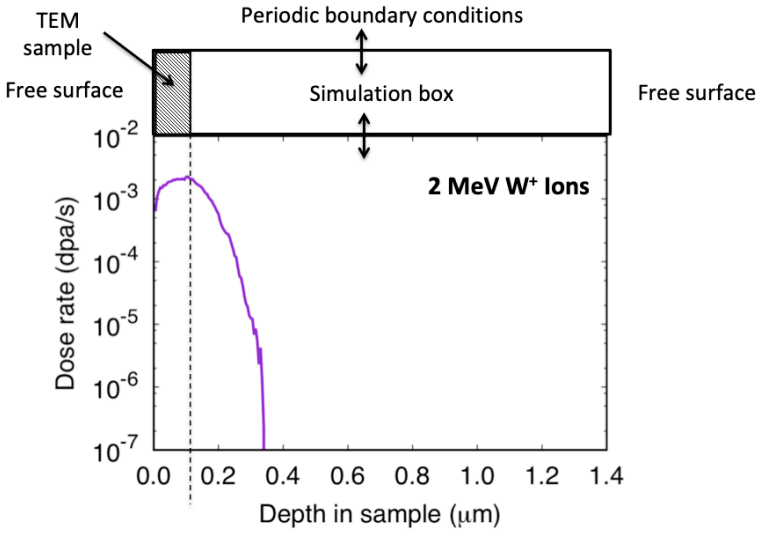

Fig 1 – Profile of dose rate as a function of depth as estimated by SRIM [25]. Our OKMC simulation box, and the depth of the TEM sample, are illustrated to scale on the top for comparison.

2.3 Post-irradiation analysis with TEM

Examples of images obtained with TEM are collected in Fig 2. From these images, the dislocation density of 4.5×10^{12} m^{-2} was calculated using a method discussed in Ref [27]. Radiation-induced defects were observed as faint dark sports homogeneously distributed in the bulk of the material. These are identified as small clusters of SIA defects, or small dislocation loops for the bigger ones. For simplicity, we do not make a qualitative distinction between these defects, and they are henceforth denoted as "loops" in what follows. The number density of the loops was calculated by direct count in 5-7 images (whose area size was 330x330 nm or 230x230 nm), divided by the corresponding volume. Their size was geometrically estimated from the TEM image. Both findings are summarized in Fig. 3:

- At 0.02 dpa, the overall number density is $8.4 \pm 1 \times 10^{21}$ m^{-3}, and the average size is 2.5 ± 0.08 nm.
- At 0.15 dpa, the number density is $9.5 \pm 1 \times 10^{21}$ m^{-3}, and the average size is 1.65 ± 0.08 nm.
- At 1.2 dpa, the number density is $52.2 \pm 5 \times 10^{21}$ m^{-3}, and the average size is 2.43 ± 0.11 nm.

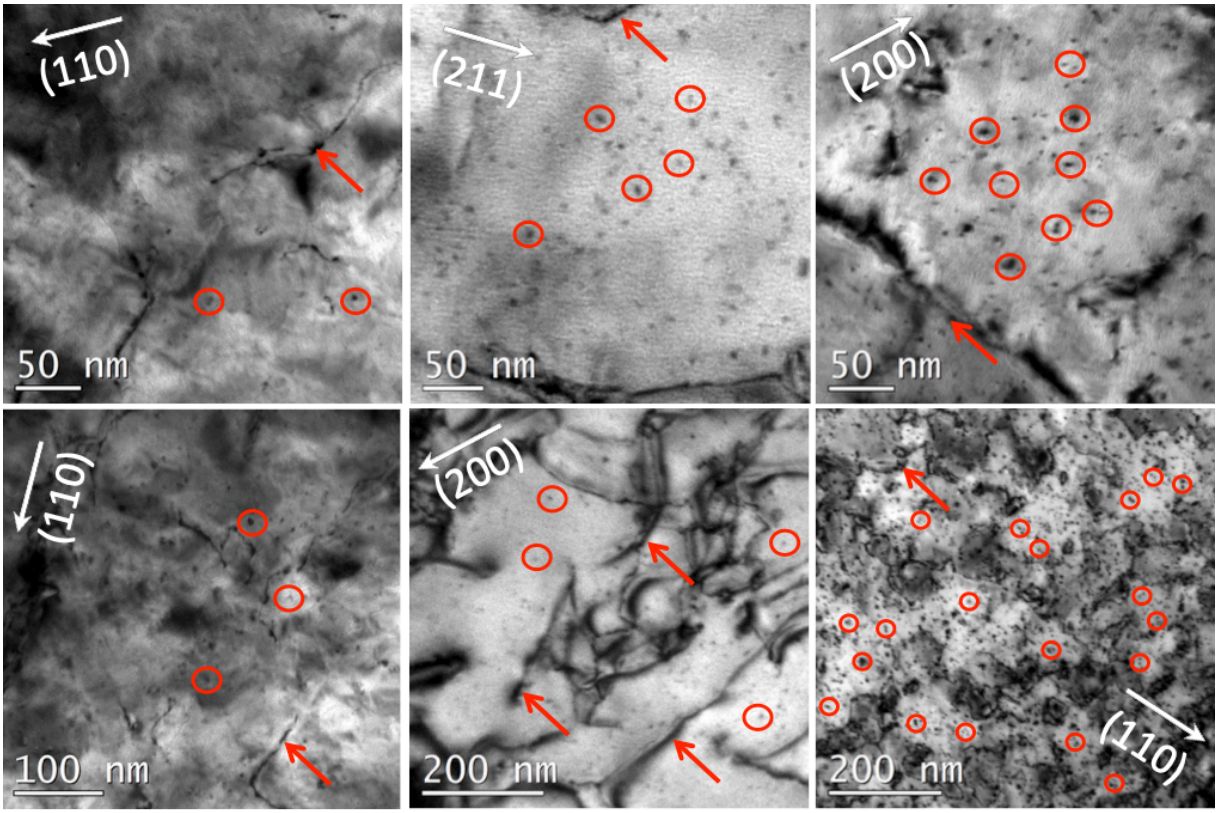

Fig 2 – Selection of images obtained with TEM at the three different doses. In these images, faint dark spots (some of them marked by red circles) are identified as dislocation loops. Some dislocation lines are marked by red arrows.

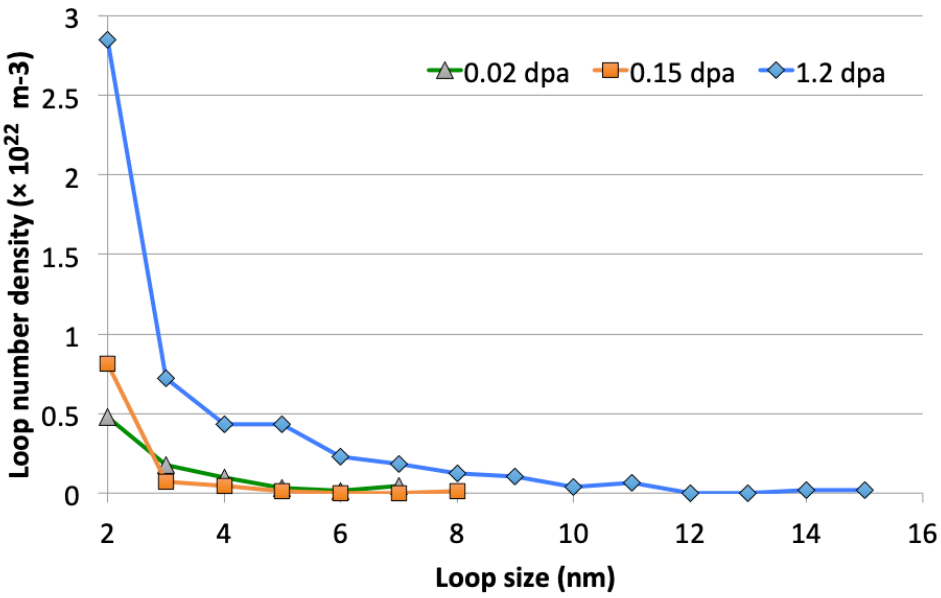

Fig 3 – Summary of the information deduced from the TEM images about SIA loops.

We see, in Fig. 3, that the number density of dislocation loops remained constant between 0.02 dpa and 0.15 dpa, but significantly increased at 1.2 dpa. The size

distribution is, however, similar between the 3 doses. New loops were therefore seeded between 0.15 dpa and 1.2 dpa, but not significant amount of coalescence seems to have taken place.

2.4 Chemical analysis with SIMS

Carbon depth profiles were measured with Secondary Ion Mass Spectrometry (SIMS) using a double focusing magnetic sector instrument VG Ionex IX-70S. A 12 keV Cs^+ primary beam was used. Samples were in a vacuum of 10^{-9} mbar. The current of the primary beam was 750 nA and the beam was raster-scanned over an area of 280 ×290 μm^2. A 10% electronic gate was used to avoid crater wall effects. After the SIMS measurements, the depths of the craters were measured with a profilometer. Typical sputter rate was 0.6 nm/s.

The left panel in Fig. 4 shows that the unirradiated sample has a flat profile with depth for C. On the contrary, irradiated samples in the right panel in Fig. 4 reveals a surface peak for C, and a clearly lower concentration in the bulk. In addition, the C concentration near the surface for samples with irradiation dose of 0.15 dpa and 1.2 dpa is significantly higher than in the sample irradiated at 0.02 dpa. At the relevant depth where the TEM sample is analyzed (first 100-150 nm) the C amount has increased by more than an order of magnitude between 0.02 and 0.15-1.2 dpa. This indicates a C injection during irradiation, from the free surface.

It is worth noting that, because of a time gap between the different SIMS measurements, quantitative results obtained for the non-irradiated sample are not directly comparable with those obtained from the irradiated samples. Due to unavoidable changes in the exact SIMS settings, and the possible changes of residual C atoms in the vacuum, both panels in Fig. 4 can only be qualitatively compared. Measurement within the right panel in Fig. 4 are, nevertheless, directly comparable in magnitude. For clarity, the left panel was thus plotted in arbitrary units.

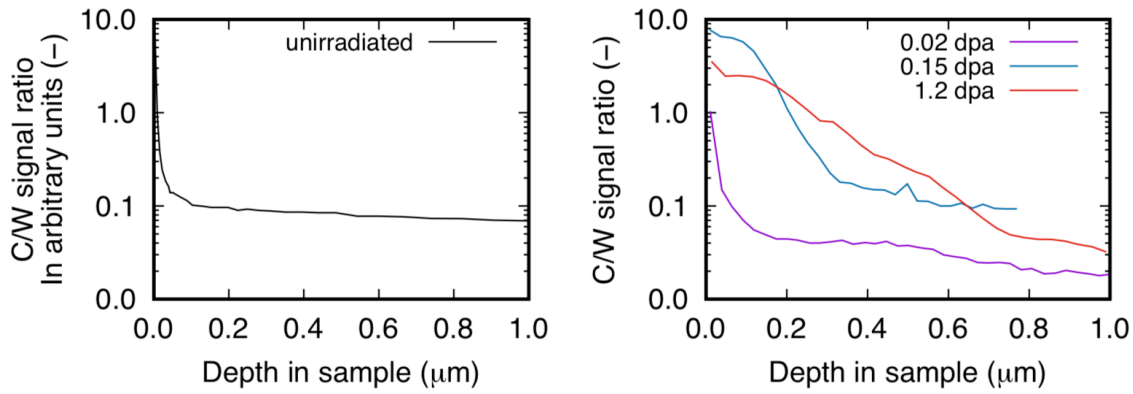

Fig 4 – SIMS measurements, expressed in a dimensionless signal ratio between C and W. (left) Qualitative evolution with depth in the non-irradiated sample; (right) Quantitative evolution with depth in the irradiated samples.

3 Modeling with object kinetic Monte Carlo

In our previous work [10], we studied the mechanism of formation of TEM-visible loops (≥ 2 nm in size) during 2 MeV self-ion irradiation experiments, in the range of 300°C to 750°C. The conclusion stemming from our OKMC model was that these loops are, for the most, directly created during the primary damage of irradiation. Molecular dynamics studies [28,29], which serve as input for our model, have indeed shown that loops ≥ 2nm are found within the debris of some of the atomic collision cascades: those triggered after a high enough transfer of kinetic energy to the primary knock-on atom (PKA), above 100 keV. In the absence of impurities in the material like C, or solute atoms like Re and Os, those loops are quickly eliminated because of their very small migration energy and their one-dimensional diffusion character [30]. Their most probable fate is to diffuse towards sinks in the microstructure, i.e. the network of dislocations and the grain boundaries, if they are not annihilated by vacancy defects on their way. Nevertheless, a small proportion of the loops find a C impurity, which acts as a trap keeping it in the bulk of the material. Calculations with density functional theory (DFT) evidenced that the magnitude of this trapping is as high as 0.72 eV for the single SIA [10]. Hypothetically, any SIA loop would exhibit a higher binding energy with single C atoms, as a function of their size. Therefore, in the irradiation experiment performed in this work, at room temperature: (1) the rate of loops creation is likely governed by the source term from the irradiation with self-ions, constant with time; (2) assuming the temperature is 20°C, we can calculate that the average time for unbinding exceeds the time of the experiment (1.2 dpa or 615 s at 2×10^{-3} dpa/s) if the binding energy is larger than 0.90 eV. Clearly, most the SIA defects can be assumed to be definitely immobile once they find a C impurity, unless they are small.

The above-described scenario can explain why the number density of loops has significantly increased between 0.15 dpa and 1.2 dpa, but not between 0.02 dpa and 0.15 dpa because this time interval is too short. Other factors must be taken into account, however: (1) the presence of the free surface near the studied volume, which acts as a sink for mobile SIA defects; (2) the creation of vacancy-type defects in the bulk, together with SIA, within the debris of atomic collision cascades. Their effect is to annihilate the migrating SIA defects in the bulk; (3) the initial content in C impurities and its increase during the experiment, as evidenced in Fig. 4. Additionally, the uncertainties in the model must be rationalized, via an adequate parametric study.

For that purpose, in the remaining of this section we apply our OKMC model to study the evolution of the microstructure, in the relevant conditions for the experiment performed in this work. We start, in section 3.1, to recall the most important information about our OKMC model, and its specific application in this work. Then, in section 3.2, the results are presented and discussed.

3.1 Model description and assumptions

Readers are directed to Ref. [9,10] for a complete description of our OKMC model, applied to W materials. Concisely, the main features of the model are:

- The simulation box, as depicted in Fig. 1, has a size of 150 a_0 × 160 a_0 × 4000 a_0, i.e. 62.6 nm × 66.7 nm × 1670 nm. Free surfaces are assumed on the boundaries

of the Z direction, and the irradiation takes place from the left hand side in Fig. 1. Periodic boundary conditions are applied on the X and Y directions. Large microstructure features like grain size and dislocation density are included as sink strength.

- As previously mentioned, irradiation is described by the injection of pre-calculated libraries of debris from atomic collision cascades obtained from molecular dynamics (MD) [28,29]. The spectrum of kinetic energy associated to the PKA was estimated using MARLOWE [31,32].
- Once injected, point-defects and their clusters are associated to migration and dissociation events. Regarding the low temperature in this work, vacancies and C defects can be assumed to be immobile, because of their high migration energy (respectively, 1.66 eV and 1.46 eV). The only events that can take place are:
    - Migration of a SIA defect towards a first-nearest-neighbor position. The migration energy is as low as 0.01 eV, and the attempt frequency linearly decreases with the size of the loop.
    - After each migration event, a probability for being sunk at a microstructure defect is considered. The probabilities are calculated from the theoretical formulas for the network of dislocations, and the grain boundaries.
    - If not sunk, the neighborhood of the SIA defect is searched for candidate defects interacting with it. Recombination with vacancy defects, and coalescence with other SIA defects, are applied immediately. Another possible interaction is with C impurities, assumed to be immobile and spherical traps.
    - If trapped by a C impurity, the migration energy of the loop is augmented by the assumed trapping energy.

An essential input parameter to the OKMC model is therefore the concentration of C impurities in the bulk of the material. It should be noted that the best choice for the model is not necessarily directly obtained from the chemical composition of the alloy, or in this work, the direct measurement with SIMS as reported in Fig. 4. Our experience (see discussions in Ref. [9,10]) showed that these numbers are too excessive for the model to make relevant predictions. In other words, according to our OKMC model, the effective concentration $C_C^{(eff)}$ of C impurities, acting as a trap for migrating point-defects, is lower than the overall C content in the material. An explanation is that C may be found in clusters, preferably in vacancy clusters or nano-voids, and is also favorable to cluster in grain boundaries and dislocations. In consequence, our approach in previous work was to perform a parametric study, and find the best-suited value for the concentration of C. In this work, regarding the SIMS evidence, we assume that the effective concentration increases with the dose:

$$C_C^{(eff)} = C_0 \ + d \cdot \bar{C}(d) \qquad (1)$$

Here, C_0 is the assumed initial concentration at the beginning of irradiation. $\bar{C}$ is the assumed injection rate as a function of the dose d. SIMS results suggest that this rate is not constant with dose, as the observed concentration did not change significantly from 0.15 to 1.2 dpa. Since the TAMIA tandem beam sweeps the implantation surface, the C injection is expected to be globally proportional to the dose, even though some inhomogeneity occurs on the implantation surface. It is worth noticing, in Fig. 4, the

large discrepancy of SIMS measurement between the unirradiated sample and the lowest dose deep in the sample. This suggests that C concentration also depends on location in the sample, e.g. from one grain to another.

For simplicity, we assume a constant rate of C injection from the beginning of irradiation (d = 0), homogeneous in the whole simulation box, but only active up to a given dose $d_{I,Max}$:

$$\bar{C}(d) = \bar{C} \text{ if } d \leq d_{I,Max} \quad (2)$$

$$= 0 \quad \text{if } d > d_{I,Max} \quad (3)$$

If one assumes that C injection is constant in time, a logical choice for $d_{I,Max}$ would be 1.2 dpa, i.e., the end of our irradiation experiment. However, the SIMS results in Fig. 4 shows a more complex profile, that apparently depends on the depth in the sample, and can get saturated as early as 0.02 dpa. For that reason, several values for $d_{I,Max}$ are tried in the next section.

Next, we define as $E_{C-L}^{(bind)}$ the binding energy between a C impurity and a loop (characterized by the number n_I of SIA that compose it) in the following way:

$$E_{C-L}^{(bind)} = 0.72eV + (0.9eV - 0.72eV)\frac{(n_I - 1)}{(n_I - 1)} \quad (5)$$

Here, the value 0.72 eV is the limiting case of the single SIA (n_I = 1), and 0.9 eV corresponds to a permanent trapping in this experiment (irradiation at 20°C during 615 seconds). We denote as n_I the loop size that reaches that value. In this work, we assumed n_I = 7, 19, 37, 55 or 91, corresponding to perfect hexagonal configurations. It should be noted that Eq. 5 performs a linear interpolation with n_I. This choice is justified for the sake of simplicity and because of the small size of the loops involved.

3.2 Results and discussion

To start, we performed OKMC simulations assuming a constant concentration of C though time, ignoring injection: $\bar{C}$ = 0 and $d_{I,Max}$ = 0. Results are shown in Fig. 5, assuming C_0 = 1 appm to 10 appm, and n_I = 19. We see that the OKMC simulations do not provide realistic results. First of all, the number density of loops saturates at an early dose < 0.1 dpa, and therefore, the experimental trend cannot be reproduced with a constant concentration of C: it should be 5 appm (or 3.1×10^{23} m^{-3}) to catch the low dose measurement, but as high as 15 appm (or 9.4×10^{23} m^{-3}) to catch the higher dose measurement. This early saturation can be explained by the high increase in number density of vacancy defects. From 0.1 dpa, it is as high as 10^{26} m^{-3}, i.e., 2 orders of magnitudes higher than the assumed C concentration. Newly created loops during atomic collision cascades have therefore much more chances to be annihilated by a vacancy defect, instead of being trapped by a C impurity. Secondly, the predicted average

size of the loops is largely overestimated. This suggests that the magnitude of trapping is too large. Indeed, bearing in mind that loops are 1-D migrating defects, their direct coalescence in the bulk is highly improbable. Instead, once immobilized by a C impurity, loops become a sink for migrating SIA defects, and can thereby grow by absorbing them. Consequently, the large increase in the loops size can only be prevented by reducing the binding energy between the C and the loops, i.e., increasing n_I in Eq. 5.

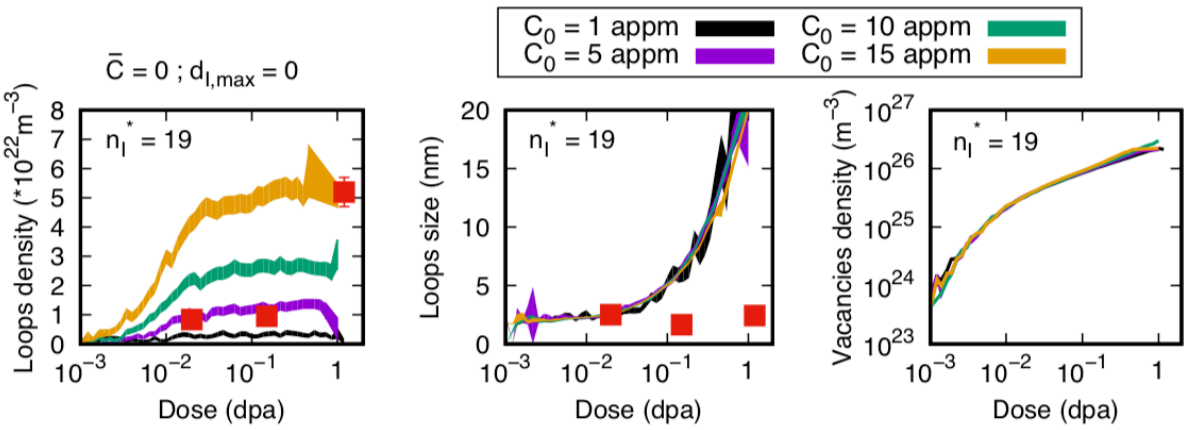

Fig 5 – Results derived by the OKMC model (lines), compared to the TEM experimental evidence (red squares). Both the loop number density (left) and the loops average sizes (right) are plotted. Different series denote the assumed effective concentration of C in the material (from 1 appm to 15 appm), assumed constant through all the irradiation.

Next, simulations were performed assuming a constant rate of C injection, assuming $d_{I,Max}$ = 0.1 dpa. Considering the results shown in Fig. 5, it seems appropriate to chose an initial concentration of C_0 = 5 appm. The obtained results, varying n_I , are shown in Fig. 6. Once again, the obtained results are not fully realistic, because the right trends are predicted for the number density of loops. Noticeably, it is found to increase while C injection is active, but then it starts decreasing afterwards. It is also interesting to note that increasing n_I has the dual effect to reduce the number density of loops after 0.1 dpa, and to noticeably reduce the average size of the loops. This can be explained in the following way:

- From 0 to 0.1 dpa, the continuous injection of C impurities has the effect to provide an increasing probability of trapping for the loops created during irradiation. Therefore, the number density of TEM-visible loops in the bulk increases. At the same time, their average size does not increase significantly, highlighting that no significant amount of coalescence takes place.
- After 0.1 dpa, the injection of C has been stopped in the simulation. Similarly to the above discussion of the results shown in Fig. 5, the number density of surviving loops does not increase any more. Their fate depends on the assumed magnitude for the binding energy:
    - If n_I =19 (which corresponds to 1.1 nm loops), the number density of loops remains constant, because the C traps are strong enough to keep all of them immobile. Their average size therefore increases with the dose, because of the coalescence with migrating SIA defects, similarly to the above-discussion from the results in Fig. 5.

- If n_I = 37 (which corresponds to 1.6 nm loops), smaller loops can unbind from the C impurities, which reduces their number densities while the average size if not significantly affected.
- If n_I = 55 (which corresponds to 1.9 nm loops), increasingly large loops can unbind from C impurities. The consequence is that, eventually, no bigger loops are ever formed.

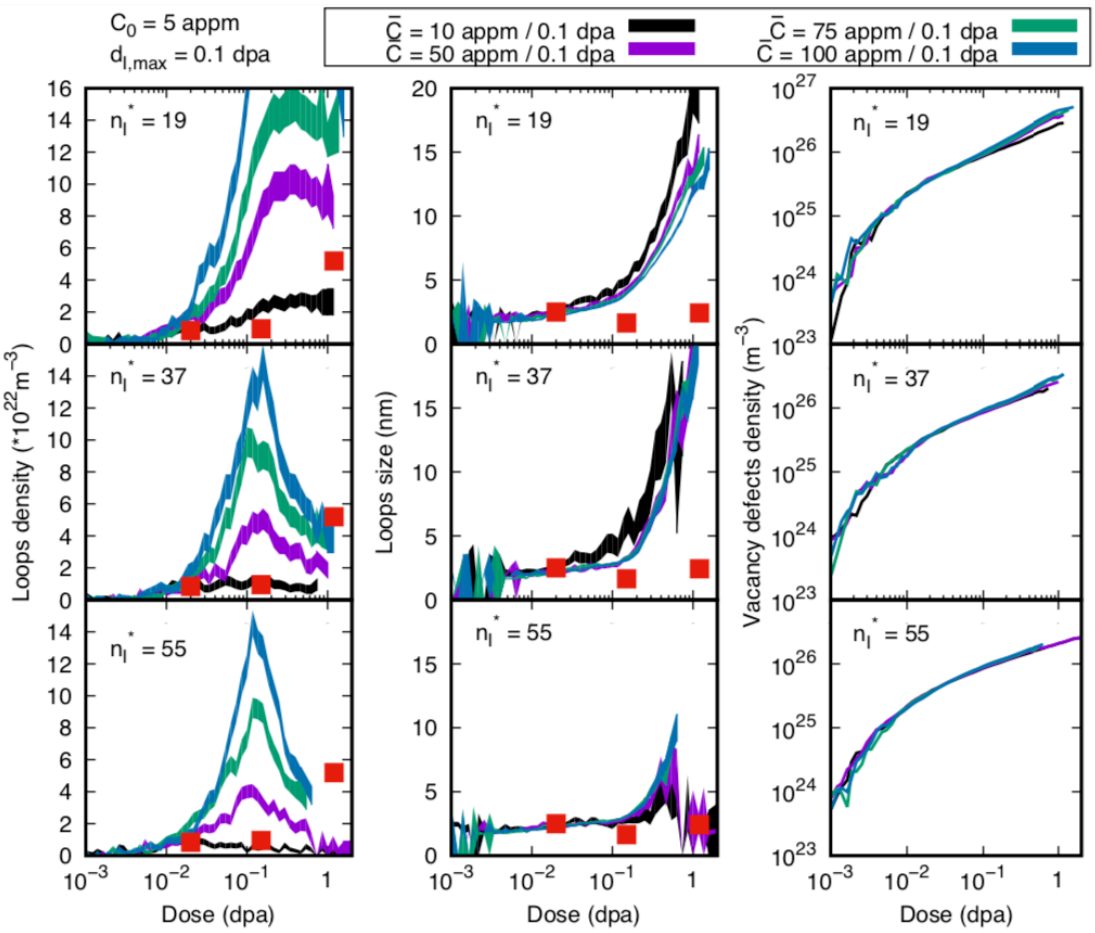

Fig 6 – Results derived by the OKMC model (lines), compared to the TEM experimental evidence (red squares). Different series denote the assumed rates of injection of C impurities in the material, all within the first 0.1 dpa only. From top to bottom, the assumed magnitude of binding between loops and C impurities is decreased (increasing n_I in Eq. 1).

Finally, simulations were performed assuming a constant rate of C injection, assuming $d_{I,Max}$ = 1 dpa and C_0 = 5 appm. The obtained results, varying n_I , are shown in Fig. 7. We see that the results of the OKMC model are realistic. Both the number density of loops, and their average size, follow the same trend as the experimental evidence, provided that $n_I \geq 37$ and $\acute{C} \geq 150$ appm/dpa. The size distribution of loops is compared in Fig. 8.

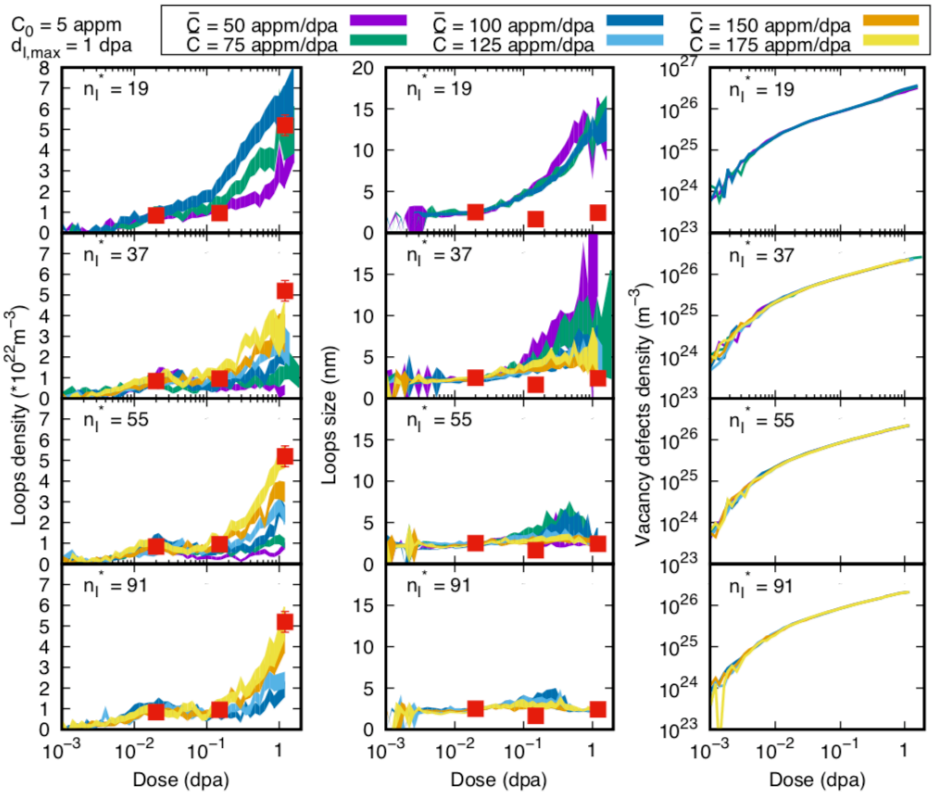

Fig 7 – Results derived by the OKMC model (lines), compared to the TEM experimental evidence (red squares). Different series denote the assumed rates of injection of C impurities in the material, all within 1 dpa. From top to bottom, the assumed magnitude of binding between loops and C impurities is decreased (increasing n_I in Eq. 1).

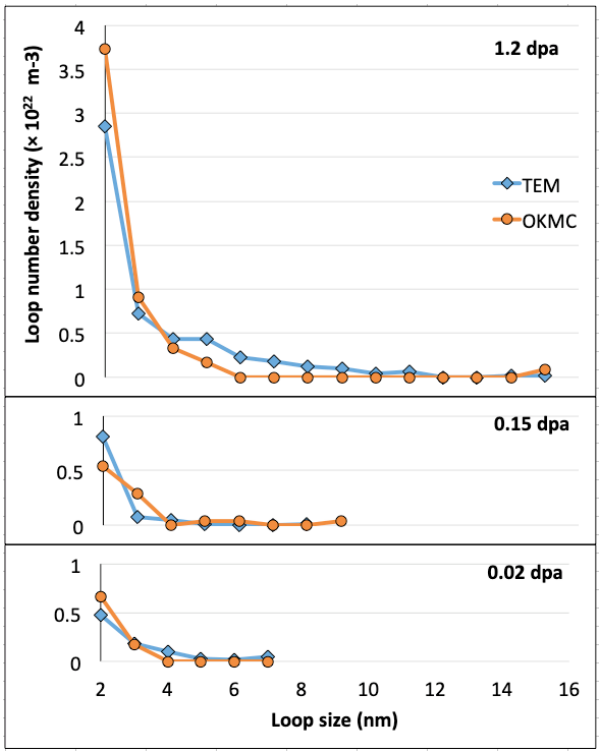

Fig 8 – Results derived by the OKMC model compared to the TEM experimental evidence for the size distribution of SIA loops.

4 Summary and conclusions

In this work, we combined an experimental and a computational approach to study the interaction between SIA defects and C impurities. For tungsten materials, room temperature ensures a complete immobility of vacancy defects and foreign impurities like C, while SIA defects remain highly mobile. As expected, TEM measurements revealed the formation of small SIA loops in all samples, including the one irradiated up to a low dose of 0.02 dpa. Surprisingly, however, we found that the number density of the loops evolved in a non-monotonous manner, because it suddenly increased between 0.15 and 1.2 dpa. Bearing in mind the well-known issue of impurities injection generally associated to ion irradiation setups [19-23], we conducted SIMS measurements on our irradiated samples. They suggested that they were likely contaminated by C injection.

In order to rationalize those experimental findings, we applied our OKMC model to simulate the same irradiation condition. We performed a parametric study for what concerns C-SIA interactions, achieving the best matching between the predictions and TEM evidence. This was obtained assuming a rate of C injection that somehow differs from the experimental one, however. This can be regarded as the effect of the remaining uncertainties in the input to the model, which can have several origins: (a) the exact magnitude of binding between C defects and SIA defects; (b) the influence of long-range elastic interactions between SIA defects, not accounted for in the present model; (c) the inhomogeneity of the C injection in the real experiment, not faithfully accountable in the model without additional assumptions. Nevertheless, our results with the OKMC model clearly concluded that the progressive injection of C impurities during the irradiation is a likely factor that explains the observed evolution with dose of the loops density.

Acknowledgements

This work has been carried out within the framework of the EUROfusion Consortium and has received funding from the Euratom research and training programme 2014-2018 under grant agreement No 633053. The views and opinions expressed herein do not necessarily reflect those of the European Commission.

References

[1] T.Hirai et al., Use of tungsten material for the ITER divertor, Nucl. Mater. Energy **9** (2016) 616-622.

[2] V. Barabash, G. Federici, M. Rödig, L.L. Snead and C.H. Wu, Neutron irradiation effects on plasma facing materials, J. Nucl. Mater. **283-287** (2000) 138-146.
[3] L.K. Keys and J. Motef, Neutron irradiation and defect recovery of tungsten, J. Nucl. Mater. **34** (1970) 260-280.
[4] I.V. Gorynin et al., Effects of neutron irradiation on properties of refractory metals, J. Nucl. Mater. **191-194 A** (1992) 421-425.
[5] J. Matolich, H. Nahm and J. Motef, Swelling in neutron irradiated tungsten and tungsten-25 percent rhenium, Scr. Metall. **8** (1974) 837-841.
[6] S. Brezinsek et al, Plasma-wall interaction studies within the EUROfusion Consortium: progress on plasmafacing components development and qualification, Nucl. Fusion 57 (2017) 116041.
[7] S. I. Alexandrov, I.V. Gorynin, Metallovedenie **22** (1979) 35.
[8] J.M. Steichen, Tensile properties of neutron irradiated TZM and tungsten, J. Nucl. Mater. **60** (1976) 13-19.
[9] N. Castin, A. Bakaev, G. Bonny, A.E. Sand, L. Malerba, D. Terentyev, On the onset of void swelling in pure tungsten under neutron irradiation: An object kinetic Monte Carlo approach, J. Nucl. Mater. **493** (2017) 280-293.
[10] N. Castin, G. Bonny, A. Bakaev, C.J. Ortiz, A.E. Sand, D. Terentyev, Object kinetic Monte Carlo model for neutron and ion irradiation in tungsten: Impact of transmutation and carbon impurities, J. Nucl. Mater. **500** (2018) 15-25.
[11] J. Marian et al., Recent advances in modeling and simulation of the exposure and response of tungsten to fusion energy conditions, Nucl. Fusion **57** (2017) 092008.
[12] C.S. Becquart, C. Domain, U. Sarkar, A. De Backer, M. Hou, Microstructural evolution of irradiated tungsten: Ab initio parameterisation of an OKMC model, J. Nucl. Mater. **403** (2000) 75-88.
[13] X. Yi, M.L. Jenkins, K. Hattar, P.D. Edmondson, S.G. Roberts, Characterisation of radiation damage in W and W-based alloys from 2 MeV self-ion near-bulk implantations, Acta Mater. **92** (2015) 163-177.
[14] F. Ferroni, W. Yi, K. Arakawa, S.P. Fitzgerald, P.D. Edmondson, S.G. Roberts, High temperature annealing of ion irradiated tungsten, Acta Mater. **90** (2015) 380-393.
[15] T. Hwang, M. Fukuda, S. Nogami, A. Hasegawa, H. Usami, K. Yabuuchi, K. Ozawa, H. Tanigawa, Effect of self-ion irradiation on hardening and microstructure of tungsten, Nucl. Mater. Energy **9** (2016) 430-435.
[16] T. Tanno, M. Fukuda, S. Nogami, A. Hasegawa, Microstructure Development in Neutron Irradiated Tungsten Alloys, Mater. Trans. **52** (2011) 1447-1451.
[17] H.H. Neely, D.W. Keefer, A. Sosin, Electron Irradiation and Recovery of Tungsten Phys. Stat. Sol. **28** (1968) 675-682.
[18] L. K. Keys, J. P. Smith, J. Moteff, High-Temperature Recovery of Tungsten after Neutron Irradiation, Phys. Rev. **176** (1968) 851.
[19] L. Shao, J.G. Gigax, D. Chen, H. Kim, F.A. Garner, J. Wang, M.B. Toloczko, Standardization of accelerator irradiation procedures for simulation of neutron induced damage in reactor structural materials, Nucl. Instrum. Meth. Phys. Res. B **490** (2017) 251–254.
[20] J.G. Gigax, H. Kim, E. Aydogan, F.A. Garner, S.A. Maloy, L. Shao, Beam-contamination-induced compositional alteration and its neutron-atypical consequences in ion simulation of neutron-induced void swelling, Mater. Res. Lett. **5** (2017) 478–485.

[21] G. Was, S. Taller, Z. Jiao, A.M. Monterrosa, D. Woodley, D. Jennings, T. Kubley, F. Naab, O. Toader, E. Uberseder, Resolution of the carbon contamination problem, Nucl. Instrum. Meth. Phys. Res. B **412** (2017) 58-65.
[22] A.M. Monterrosa, D. Woodley, Z. Jiao, G.S. Was, , J. Nucl. Mater. **509** (2018) 722-735.
[23] J. G. Gigax, H. Kim, E. Aydogan, L.M. Price, X. Wang, S.A. Maloy, F.A. Garner, L. Shao, Impact of composition modification induced by ion beam Coulomb-drag effects on the nanoindentation hardness of HT9, Nucl. Instrum. Meth. Phys. Res. B **444** (2019) 68-73.
[24] A.Dubinko, D.Terentyev, A.Bakaeva, K.Verbeken, M.Wirtz, M.Hernández-Mayoral, Evolution of plastic deformation in heavily deformed and recrystallized tungsten of ITER specification studied by TEM, Int. Journal of Refractory Metals and Hard Materials **66** (2017) 105-115.
[25] J.F. Ziegler et al., SRIM - The Stopping and Range of Ions in Matter, available at http://www.srim.org/index.htm#HOMETOP.
[26] D.R. Mason, X. Yi, M.A. Kirk and S.L. Dudarev, Elastic trapping of dislocation loops in cascades in ion-irradiated tungsten foils, J. Phys.: Condens. Matter **26** (2014) 375701.
[27] T. W. Butler, On the determination of dislocation densities. 1969, Annapolis.
[28] A.E. Sand, S.L. Dudarev, K. Nordlund, High-energy collision cascades in tungsten: Dislocation loops structure and clustering scaling laws, Europhys. Lett. **103** (2013) 46003.
[29] A. Sand, K. Nordlund, S. Dudarev, Radiation damage production in massive cascades initiated by fusion neutrons in tungsten, J. Nucl. Mater **455** (2014) 207-211.
[30] T.D. Swinburn, P-W Ma and S.L. Dudarev, Low temperature diffusivity of self-interstitial defects in tungsten, New J. Phys. **19** (2017) 073024.
[31] M.T. Robinson, I. Torrens, Computer simulation of atomic-displacement cascades in solids in the binary-collision approximation, Phys. Rev. B **9** (1974) 5008.
[32] M.T. Robinson, Slowing-down time of energetic atoms in solids, Phys. Rev. B **40** (1989) 10717.